

Static dynamics approach to relaxation modes and times for deformed polymers

Roland Rzehak

Institut für Festkörperforschung, Forschungszentrum Jülich, D-52425 Jülich, Germany

Walter Zimmermann

Theoretische Physik, Universität des Saarlandes, D-66041 Saarbrücken, Germany

(Received 28 January 2003; published 26 August 2003)

We discuss relaxation of conformational fluctuations around deformed polymer states. To this end, Brownian dynamics simulations of bead-spring models including a finite extensibility of the springs as well as excluded volume and hydrodynamic interactions between the beads have been performed. Complete spectra of relaxation times as well as corresponding relaxation modes are obtained from the simulation data by applying the *static dynamics* formalism, which rigorously describes the initial decay of correlations between the bead positions. As shown here, this procedure amounts to using a generalized Rouse-Zimm-like model which is governed by *linear* effective equations of motion having the same initial decay of correlations as the full nonlinear bead-spring model used in the simulations. In thermal equilibrium, the well-known scaling laws in the presence of excluded volume and hydrodynamic interactions between the beads are recovered, but, in addition, the *static dynamics* method also yields numeric values for the nonuniversal prefactors of the respective laws. The method is equally applicable to a broad range of problems, where the polymer is deformed by the action of flows or forces. Two examples of recent interest are considered: a tethered polymer pulled at its free end and one which is stretched by a uniform flow. It is shown that in both cases, the relaxation process is dominated by a finite extensibility of the springs.

DOI: 10.1103/PhysRevE.68.021804

PACS number(s): 36.20.Ey, 05.40.Jc, 83.10.Mj, 47.50.+d

I. INTRODUCTION

The slow internal dynamics of long polymer chains is the origin of the viscoelasticity of dilute polymer solutions [1–6]. The resulting flow phenomena encompass surprising and spectacular effects such as turbulent drag reduction [7–9] or elastic turbulence [10]. While many of these phenomena have been known for a long time already, their understanding is still far from complete. A central quantity used in attempts to advance this understanding on a microscopically founded basis is the spectrum of polymer relaxation times.

In weak flows, the polymers are not disturbed much from their coiled equilibrium conformation, hence, their dynamics is well described by the *equilibrium* relaxation spectrum. The latter can be calculated from bead-spring polymer models [11–15] and a reasonable agreement with experimental data is achieved. Thus restricting to weak flows, the linear viscoelastic model of rheology [1,2] provides a well founded continuum description of the polymer solution.

A significant polymer deformation is expected according to the so-called time criterion [16] when the inverse local shear or elongation rate κ^{-1} is shorter than the longest polymer relaxation time. Since the latter is conformation dependent, because of hydrodynamic back-flow, it was argued that a hysteretic transition between a coiled and a stretched polymer conformation may occur upon varying κ [17,18]. Based on a similar argument, a truncation of the turbulent cascade was put forward as a qualitative explanation of the turbulent drag reduction phenomenon [19]. To also obtain rheological predictions in such strong flows, phenomenological dumbbell models have been proposed as a kind of minimal description of an extensible object [20–23], in which a

conformation-dependent relaxation time is used to model the polymer response.

More recently, the polymer deformation has been investigated extensively for two simple model situations: a polymer pulled at the ends and a tethered polymer subjected to a uniform flow. Experimentally, both situations are realized by using DNA as a model polymer which can be manipulated with the aid of optical tweezers and which can be observed by fluorescence microscopy [24–27]. Specifically for the polymer pulled at the ends, the relaxation times and modes have been measured directly [27].

Theoretical predictions of the polymer elongation and relaxation times have been obtained mainly through the blob model, for the polymer pulled at the ends in Refs. [14,28,29] and for the polymer in uniform flow in Refs. [30–33]. The blob model is very appealing because scaling laws for both global and local properties characterizing the deformation as well as the dynamics of the polymer can be derived analytically even in the presence of excluded volume and hydrodynamic interactions.

Calculations for bead-spring models representing the many degrees of freedom of a polymer chain more faithfully have been carried out at different levels of approximation for the interactions between the beads. The end-pulled case is the subject of Refs. [34,35], while Refs. [36–39] consider the uniform flow case. In comparison to the simulation data, the basic assumptions of the blob model have been verified and some improvements have been suggested [38–41]. The relaxation times have been estimated specifically for the end-pulled case in Refs. [34,35]. For the uniform flow case, a calculation based on the blob model has been carried out in Refs. [32,55]. Preliminary results using the *static dynamics* approach have been given in Ref. [42]. In the present work,

this method, which allows for a systematic evaluation of polymer relaxation times and modes from simulation data for bead-spring models, is discussed in detail. As an illustrative application we compare the two prototypic situations of a tethered polymer pulled at the end and one which is subjected to a uniform flow. In both cases, the relaxation times show a qualitatively similar behavior, but the corresponding modes have a rather different shape.

The polymer relaxation spectrum can be calculated analytically only for the simplest polymer models, namely, those of Rouse [11] and Zimm [12,13]. Both these models share the feature that they yield linear equations governing the motion of the polymer. Hence, a complete analytic solution can be obtained in terms of independently evolving relaxation modes which decay exponentially with a certain relaxation time. For more realistic nonlinear polymer models, modern simulation techniques allow us to solve the equation of motion numerically. When similar information on the dynamics as for the linear models is sought, however, a fundamental difficulty is encountered [14,23,43]: the nonlinearity leads to a coupling of modes and fully independently relaxing modes, as in the linear case, do not exist.

A common way to deal with this situation is to simply assume that the amplitudes of the Rouse modes retain their significance for the relaxation of the polymer chain even for nonlinear polymer models [44,45]. This assumption may be reasonable for a polymer in thermal equilibrium, but is rather unlikely to hold for strongly deformed polymers subjected to external forces or flows. Even if one accepts the premise of using the Rouse modes, the relaxation times then have to be determined from an exponential fit to the time series of the Rouse amplitudes, which is tedious and error prone so that, in practice, only the few longest relaxation times can be obtained in this way.

Another approach which aims at the relaxation spectrum directly without reference to a set of modes is to apply an inverse Laplace transform to a single time series of some observable such as the distance between the ends of the polymer [24]. Here, however, the result generally depends on the choice of the observable. Furthermore, the inversion is an ill-conditioned problem due to the presence of noise in the data and requires the use of special regularization techniques [46,47]. The results then, in general, depend strongly on the regularization parameter.

Here, we analyze a way to determine the relaxation spectrum for nonlinear polymer models which is linked rigorously to the initial decay of correlations in the motion of the polymer segments. This method is similar in spirit to an earlier work that made an attempt to approximate dynamical quantities in terms of static averages for which the term *static dynamics* has been coined [48]. In contrast to these previous works, which have focused on determining various transport coefficients [49,50], we here aim directly at the calculation of relaxation times and also obtain a corresponding set of relaxation modes [42]. In this way a direct comparison to calculations based on blob models [32] and to recent experiments measuring both relaxation times and modes [25,27] becomes possible, see Ref. [55]. The *static dynamics* approach to relaxation times and -modes employs

a linearization of the time evolution of the correlation function about the initial state [15]. An agreement with scaling theories that do not rely on the mode concept shows that this approximation captures the essence of the dynamics of fluctuations of the polymer conformation in a statistically steady state. The modes obtained are a natural generalization of the linear eigenmodes in that their initial decay is *uncorrelated*. They essentially describe the dynamics of a generalized Rouse-Zimm-like model [51]. The *static dynamics* method is particularly useful in evaluating data from numerical simulation. From practical point of view, the method is fast, easy to use, needs no adjustments of parameters or additional assumptions, and yields the complete spectrum in one sweep.

The outline of the paper is as follows. In Sec. II we consider polymer models with linear dynamics like those of Rouse [11] and Zimm [12]. For these models, the general solution is obtained analytically as a superposition of a complete set of modes which decay independent of each other. The evolution of each of these modes follows an exponential law with a certain relaxation time. An important issue is to clarify consequences of the possible noncommutability of the matrix of force constants and the mobility matrix. This is a standard result in linear algebra [52,53], and classical mechanics [54] which is summarized to prepare the stage for further development concerning nonlinear models.

In Sec. III, we turn to the *static dynamics* approach [15,42,48,55] which is based on a rigorous relation for the initial decay rate of correlations between two observables of the polymer conformation. The previous derivation of this relation [15] makes use of the Boltzmann distribution and, hence, is valid only in thermal equilibrium. We give a somewhat more general treatment, which requires only detailed balance to hold without assuming a special form of the distribution of polymer conformations. As shown in Appendix A, the detailed balance condition applies to an important class of polymer flow problems. We then generalize the previous treatment [15] to vector observables. From the discussion in Sec. II it becomes clear that there is a unique coordinate transformation which eliminates cross correlations between vector components.

In Sec. IV, the *static dynamics* method is applied to the Rouse model, and a comparison with the exact analytical solution for the discrete case is made. This allows us to assess the accuracy and the amount of data required to reduce numerical errors to an acceptable level. Since standard texts mostly consider the continuous limit, a solution for the discrete case with the same boundary conditions as used in the simulations is given in Appendix C.

In Sec. V, bead-spring polymer models including various nonlinear effects are analyzed by the *static dynamics* method under conditions of thermal equilibrium. The effects considered are a finite extensibility of the springs as well as excluded volume interactions and hydrodynamic interactions between the beads. Details of the modeling are described in Appendix B. The relaxation spectra obtained with the *static dynamics* method are shown to agree with the available scaling results.

Finally, in Sec. VI we turn to two simple nonequilibrium problems which have recently attracted a great deal of atten-

tion. Specifically, we compare a polymer chain pulled at the ends [27,34,35] to a tethered chain stretched by a uniform flow [32,36,40,55]. For the latter, a rather large database has been accumulated during a previous investigation [39]. For the former, some further simulations have been carried out showing that the modes are rather different in both cases. This indicates that care must be taken when extrapolating results between different external conditions.

II. LINEAR POLYMER MODELS

In this section we consider bead-spring polymer models which are described by a linear Langevin equation with additive noise,

$$\frac{\partial}{\partial t} \mathbf{R} = -\bar{\mathbf{H}}\bar{\mathbf{K}}\mathbf{R} + \sqrt{2k_B T \bar{\mathbf{H}}} \boldsymbol{\xi}. \quad (1)$$

Here, like for the nonlinear models detailed in Appendix B, \mathbf{R} is a supervector comprising the Cartesian components of the positions of all N beads and $\boldsymbol{\xi}$ is a Gaussian white noise with zero mean and unit variance. The mobility matrix $\bar{\mathbf{H}}$ and the matrix of force constants $\bar{\mathbf{K}}$ are both symmetric and positive. Moreover, in contrast to the models used in the simulations as described in Appendix B, we here assume both $\bar{\mathbf{H}}$ and $\bar{\mathbf{K}}$ to be independent of the polymer conformation \mathbf{R} .

Clearly, the classic models of Rouse [11] and Zimm [12] are of the above form. But more generally, $\bar{\mathbf{H}}$ may arise from averaging the true conformation-dependent mobility matrix $\mathbf{H}(\mathbf{R})$ given by Eq. (B8) with respect to the conformational distribution for a deformed polymer, so that

$$\bar{\mathbf{H}} = \langle \mathbf{H}(\mathbf{R}) \rangle. \quad (2)$$

The elements of $\bar{\mathbf{K}}$, in turn, may be considered as effective force constants defined in terms of correlations between the bead positions of a deformed polymer. By virtue of the equipartition theorem, we have

$$\bar{\mathbf{K}} = k_B T \langle \mathbf{U}\mathbf{U}^T \rangle^{-1}, \quad (3)$$

where $\mathbf{U} = \mathbf{R} - \langle \mathbf{R} \rangle$ gives the deviation of the actual bead positions from their average values.

In the presence of an external flow or force, the average bead positions $\langle \mathbf{R} \rangle$ are nonzero. However, owing to linearity \mathbf{U} may replace \mathbf{R} in Eq. (1), which we suppose from now on, i.e., Eq. (1) will be used to describe fluctuations around the average bead positions rather than the bead positions themselves. Then, the matrices $\bar{\mathbf{H}}$ and $\bar{\mathbf{K}}$, as defined by Eqs. (2) and (3), already contain the effects of an imposed flow so that the latter does not appear explicitly in the equation of motion, Eq. (1). The kinetic part of this method, embodied in the definition of $\bar{\mathbf{H}}$ in Eq. (2), is similar to the generalized Rouse-Zimm model of Ottinger [51], but here used to describe fluctuations of the polymer conformation.

Since Eq. (1) is linear, a complete solution can be obtained in terms of relaxation times and modes which solve the eigenproblem

$$\Gamma \mathbf{Q}_p \equiv \bar{\mathbf{H}}\bar{\mathbf{K}}\mathbf{Q}_p = \tau_p^{-1} \mathbf{Q}_p, \quad (4)$$

where p and all other indices appearing below run from 1 to $3N$. The eigenvalues τ_p^{-1} give the inverse relaxation times and the eigenvectors \mathbf{Q}_p are the corresponding relaxation modes. These make up the columns of a matrix \mathbf{Q} that effects a coordinate transformation in conformation space

$$\tilde{\mathbf{U}} = \mathbf{Q}^{-1} \mathbf{U}, \quad (5)$$

so that the transformed matrix

$$\tilde{\Gamma} = \mathbf{Q}^{-1} \Gamma \mathbf{Q} \quad (6)$$

becomes diagonal.

Since $\bar{\mathbf{H}}$ and $\bar{\mathbf{K}}$ in general do not commute, their product Γ is not symmetric even though $\bar{\mathbf{H}}$ and $\bar{\mathbf{K}}$ are. However, since $\bar{\mathbf{H}}$ and $\bar{\mathbf{K}}$ are positive, Eq. (4) poses a so-called generalized symmetric-definite eigenproblem [52,53], which also appears in the classical mechanics of coupled oscillators [54]. Its basic properties are summarized in the following, where summation over repeated indices will be implied. The eigenvalues are real and the eigenvectors form a complete system which, however, is not orthogonal, i.e., $Q_{pi}^T Q_{iq} \neq \delta_{pq}$. Instead, the relation

$$Q_{pi}^T \bar{\mathbf{H}}_{ij}^{-1} Q_{jq} = \delta_{pq} \quad (7)$$

holds, which together with the eigenvalue relation (4) gives

$$Q_{pi}^T \bar{\mathbf{K}}_{ij} Q_{jq} = \tau_p^{-1} \delta_{pq}. \quad (8)$$

Owing to the positivity of $\bar{\mathbf{H}}$, and hence also $\bar{\mathbf{H}}^{-1}$, the first of these may be considered as a generalized orthogonality relation [56]. Moreover, these relations express the fact that $\bar{\mathbf{H}}^{-1}$, and hence also $\bar{\mathbf{H}}$, as well as $\bar{\mathbf{K}}$ are diagonalized simultaneously, but by a congruence rather than a similarity transformation with the matrix \mathbf{Q} [12,52,53]. Therefore, these relations *do not* give the matrix elements of $\bar{\mathbf{H}}^{-1}$ and $\bar{\mathbf{K}}$ with respect to the eigenbasis \mathbf{Q}_p . The matrix elements of $\bar{\mathbf{H}}$ and $\bar{\mathbf{K}}^{-1}$, however, *do* have a simple expression in terms of the metric $Q_{pi}^T Q_{iq}$, namely,

$$\tilde{\mathbf{H}}_{pq} = Q_{pi}^{-1} \bar{\mathbf{H}}_{ij} Q_{jq} = Q_{pi}^T Q_{iq} \quad (9)$$

and

$$\tilde{\mathbf{K}}_{pq}^{-1} = Q_{pi}^{-1} \bar{\mathbf{K}}_{ij}^{-1} Q_{jq} = \tau_q Q_{pi}^T Q_{iq}. \quad (10)$$

It will be shown in the following section that the linear model with $\bar{\mathbf{H}}$ and $\bar{\mathbf{K}}$, defined by Eqs. (2) and (3), gives exactly the same initial decay as the original nonlinear model from which the averaged mobility and effective force constants have been derived.

III. STATIC DYNAMICS

For linear systems such as those considered in the preceding section, the concept of relaxation modes and times is clear-cut: the state vector \mathbf{R} representing the polymer conformation is expanded in a set of base vectors for which the dynamics becomes uncoupled. For nonlinear systems, a decomposition satisfying such a strong property is not possible in general. Thus, to exploit the power of linear methods, some approximation must be made. One such approximation that has been found particularly useful, since it allows to draw conclusions about the relaxation of two-time correlations from calculation of one-time moments only, is the so-called *static dynamics* approach [15,48]. In this section, we discuss an extension of this formalism to nonequilibrium dynamics and to vector observables. We begin by considering two scalar observables $A(\mathbf{R})$ and $B(\mathbf{R})$, which will later be taken as two components \tilde{U}_i and \tilde{U}_j of $\mathbf{U} = \mathbf{R} - \langle \mathbf{R} \rangle$ with respect to a suitable basis and we calculate the initial decay rate of correlations $\langle A(t)B(0) \rangle$. The calculation here is based on the Fokker-Planck equation equivalent to the Langevin equation (B12) rather than the Langevin equation itself.

The Fokker-Planck equation is written in the form of a conservation law as

$$\frac{\partial}{\partial t} \mathcal{P} = -\nabla \cdot \mathbf{J}[\mathcal{P}], \quad (11)$$

where the probability current $\mathbf{J}[\mathcal{P}]$ is given by [57,58]

$$\mathbf{J}[\mathcal{P}] = (\mathbf{v} + \mathbf{H} \cdot \mathbf{F}) \mathcal{P} - k_B T \mathbf{H} \cdot \nabla \mathcal{P}. \quad (12)$$

Here, \mathcal{P} is the transition probability $\mathcal{P}_{2|1}(\mathbf{R}, t | \mathbf{R}_0, 0)$ which satisfies the initial condition $\mathcal{P}_{2|1}(\mathbf{R}, t | \mathbf{R}_0, 0) = \delta(\mathbf{R} - \mathbf{R}_0)$. In the following, \mathbf{v} , \mathbf{F} , and \mathbf{H} are functions of \mathbf{R} and ∇ denotes the vector of derivatives with respect to the components of \mathbf{R} .

The time correlation $\langle A(t)B(0) \rangle$ of two observables $A(\mathbf{R}), B(\mathbf{R})$ can be calculated as

$$\begin{aligned} \langle A(t)B(0) \rangle &= \int \int A(\mathbf{R}) \mathcal{P}_{2|1}(\mathbf{R}, t | \mathbf{R}', 0) B(\mathbf{R}') \mathcal{P}_1^s(\mathbf{R}') d\mathbf{R}' d\mathbf{R}, \end{aligned} \quad (13)$$

where \mathcal{P}_1^s is the stationary distribution of bead positions. Dropping the arguments \mathbf{R} and \mathbf{R}' , the rate of change is

$$\frac{d}{dt} \langle A(t)B(0) \rangle = \int \int A \frac{\partial}{\partial t} \mathcal{P}_{2|1} B \mathcal{P}_1^s d\mathbf{R}' d\mathbf{R}. \quad (14)$$

By using the Fokker-Planck equation (11) for $\mathcal{P}_{2|1}$, we obtain

$$\begin{aligned} \frac{d}{dt} \langle A(t)B(0) \rangle &= - \int \int A \nabla \cdot [(\mathbf{v} + \mathbf{H} \cdot \mathbf{F}) \mathcal{P}_{2|1} \\ &\quad - k_B T \mathbf{H} \cdot \nabla \mathcal{P}_{2|1}] B \mathcal{P}_1^s d\mathbf{R}' d\mathbf{R}. \end{aligned} \quad (15)$$

At $t=0$, $\mathcal{P}_{2|1}(\mathbf{R}, t | \mathbf{R}', 0) = \delta(\mathbf{R} - \mathbf{R}')$, hence

$$\begin{aligned} \frac{d}{dt} \langle A(t)B(0) \rangle|_{t=0} &= - \int A \nabla \cdot [(\mathbf{v} + \mathbf{H} \cdot \mathbf{F}) B \mathcal{P}_1^s \\ &\quad - k_B T \mathbf{H} \cdot \nabla (B \mathcal{P}_1^s)] d\mathbf{R}. \end{aligned} \quad (16)$$

Partial integration results in

$$\begin{aligned} \frac{d}{dt} \langle A(t)B(0) \rangle|_{t=0} &= \int \nabla A \cdot \{ [(\mathbf{v} + \mathbf{H} \cdot \mathbf{F}) \mathcal{P}_1^s \\ &\quad - k_B T \mathbf{H} \cdot \nabla \mathcal{P}_1^s] B - k_B T \mathcal{P}_1^s \mathbf{H} \cdot \nabla B \} d\mathbf{R}. \end{aligned} \quad (17)$$

Upon introducing the current from Eq. (12), this simplifies to

$$\frac{d}{dt} \langle A(t)B(0) \rangle|_{t=0} = \int \nabla A \cdot (\mathbf{J}[\mathcal{P}_1^s] B - k_B T \mathcal{P}_1^s \mathbf{H} \cdot \nabla B) d\mathbf{R}. \quad (18)$$

The current \mathbf{J} vanishes when detailed balance holds. This is the case, of course, in equilibrium, but as shown in Appendix A it also holds for an important class of flows and forces when the hydrodynamic mobility matrix is averaged. Under this condition we recover the simple result

$$\frac{d}{dt} \langle A(t)B(0) \rangle|_{t=0} = -k_B T \langle \nabla A \cdot \mathbf{H} \cdot \nabla B \rangle, \quad (19)$$

which was obtained previously for polymers in equilibrium [15].

The initial decay may be described by a linear law where the rate constant of the relaxation is obtained as

$$\Gamma_{AB} = \frac{-\frac{d}{dt} \langle A(t)B(0) \rangle|_{t=0}}{\langle A(0)B(0) \rangle}, \quad (20)$$

when both observables decay to zero, i.e., $\langle A \rangle = \langle B \rangle = 0$.

Taking now $A = U_i = R_j - \langle R_j \rangle$ and $B = U_j = R_j - \langle R_j \rangle$, we obtain a matrix of $(3N)^2$ different relaxation rates due to cross correlations between different beads. In terms of the averaged mobility matrix $\bar{\mathbf{H}}$ and the matrix of effective force constants $\bar{\mathbf{K}}$ defined in Eqs. (2) and (3), we have

$$\Gamma_{ij} = \frac{\bar{H}_{ij}}{\bar{K}_{ij}^{-1}}. \quad (21)$$

From the analysis of linear models in Sec. II it is clear that this matrix can be made diagonal by the coordinate transformation which simultaneously diagonalizes $\bar{\mathbf{H}}$ and $\bar{\mathbf{K}}$ via congruence. This coordinate transformation in general will be nonorthogonal since $\bar{\mathbf{H}}$ and $\bar{\mathbf{K}}$ need not commute. To make the connection explicit, consider observables $A = \tilde{U}_p = \mathcal{Q}_{pm}^{-1} U_m$ and $B = \tilde{U}_q = \mathcal{Q}_{qn}^{-1} U_n$ in Eq. (20) which gives

$$\tilde{\Gamma}_{pq} = \frac{Q_{pm}^{-1} \bar{H}_{mn} (Q^{-1})_{nq}^T}{Q_{pm}^{-1} \bar{K}_{mn}^{-1} (Q^{-1})_{nq}^T}. \quad (22)$$

Inserting $\delta_{nl} = Q_{nr} Q_{rl}^{-1}$ after \bar{H}_{mn} and \bar{K}_{mn} and identifying $Q_{pm}^{-1} \bar{H}_{mn} Q_{nr}$ and $Q_{pm}^{-1} \bar{K}_{mn}^{-1} Q_{nr}$ as the matrix elements \tilde{H}_{pr} and \tilde{K}_{pr}^{-1} of \tilde{H} and \tilde{K}^{-1} in the transformed coordinates, this becomes

$$\tilde{\Gamma}_{pq} = \frac{\tilde{H}_{pr} Q_{rl}^{-1} (Q^{-1})_{lq}^T}{\tilde{K}_{pr}^{-1} Q_{rl}^{-1} (Q^{-1})_{lq}^T}. \quad (23)$$

Now by using the relations for the matrix elements of \tilde{H} and \tilde{K} from Eqs. (9) and (10) in Sec. II it is seen that the sums in the numerator and the denominator each reduce to a Kronecker δ so that

$$\tilde{\Gamma}_{pq} = \tau_p^{-1} \delta_{pq}. \quad (24)$$

In summary, the essence of the *static dynamics* approach is the use conformation-independent matrices \bar{H} , \bar{K} which are easily calculated from simulation data according to the definitions, Eqs. (2) and (3). The matrices define a generalized Rouse-Zimm model for the conformational fluctuations of the polymer. The relaxation times and modes then are calculated in a straightforward manner by numerically diagonalizing the matrix $\Gamma = \bar{H}\bar{K}$. Its eigenmodes provide relaxation modes which initially decay uncorrelated with each other. Its eigenvalues give the inverse relaxation times describing the initial decay of these uncorrelated modes.

IV. ANALYSIS OF THE ROUSE MODEL

The analytical solution of the Rouse model for a chain in thermal equilibrium with one end fixed and the other end free, as described in Appendix C, yields a relaxation spectrum

$$\tau_p^R = \frac{\zeta}{k_H} \left[4 \sin^2 \left(\frac{2p-1}{2N+1} \frac{\pi}{2} \right) \right]^{-1}. \quad (25)$$

For further discussion it will be useful to use separate indices for bead and mode numbers $i, p = 1, \dots, N$ and directions in real space $\alpha = x, y, z$. A large part of the spectrum follows a scaling law $\tau_p \propto (2p-1)^{-2}$, cf. Fig. 2. Deviations from this scaling law at large mode numbers $p \gtrsim N/2$ are due to the finite number of beads and are absent in the usual treatment [15,59], where N is assumed to be very large so that the expansion $\sin(x) \sim x$ can be employed.

The Rouse modes are special chain conformations described in the following. Because the Gaussian conformational distribution function factorizes in the three directions of real space, $\alpha = x, y, z$, the position of the i th bead, $i = 1, \dots, N$, in the mode with indices p, α may be written as a product $\mathbf{R}_{pi}^\alpha = R_{pi} \hat{\mathbf{E}}^\alpha$. Thus, as illustrated in Fig. 1 all beads are on a straight line with unit vector $\hat{\mathbf{E}}^\alpha$ and distances R_{pi}

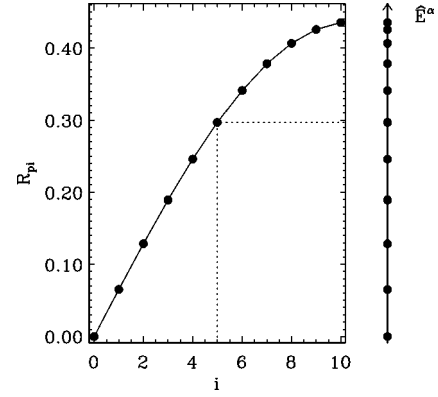


FIG. 1. Illustration of the chain conformation corresponding to the first Rouse mode ($p=1$) of a chain with $N=10$ beads. The bead positions are on a straight line with direction $\hat{\mathbf{E}}^\alpha$ (α being either x , y , or z) in real space as shown at the right side of the plot. The diagram gives the distance R_{pi} of the i th bead from the origin where the chain is fixed.

from the origin. For the distance function, the calculation in Appendix C yields N different patterns of bead spacings

$$R_{pi} = \frac{2}{\sqrt{2N+1}} \sin \left(i \frac{2p-1}{2N+1} \pi \right) \quad (26)$$

corresponding to the values $p = 1, \dots, N$.

The distance function R_{pi} is normalized according to $\sum_{i=1}^N R_{pi} R_{qi} = \delta_{pq}$ which together with the orthonormality of $\hat{\mathbf{E}}^\alpha$ in real space expresses the orthonormality of the Rouse modes in conformation space. Since there are $3N$ modes, these form a basis for the conformation space, i.e., each conformation \mathbf{R} may be expressed as a superposition $\mathbf{R} = \sum_{p=1}^N \sum_{\alpha=x,y,z} A_p^\alpha \mathbf{R}_p^\alpha$, where \mathbf{R}_p^α is the supervector, giving all bead positions for the p th Rouse mode with direction α . The mode amplitude A_p^α is a common scaling factor for the position vectors of all beads in the chain. The amplitudes A_p^α for the three coordinate directions in real space are often taken together as a vector amplitude \mathbf{A}_p .

In equilibrium, none of the three directions of a Cartesian coordinate system is distinguishable. Therefore, the spectrum of polymer relaxation times is threefold degenerate. The modes corresponding to each triplet of relaxation times differ only in their directions $\hat{\mathbf{E}}^\alpha$ in real space, while the spacing of beads along this direction is the same for all three modes in the triplet. Since all directions in space are equivalent, the directions obtained by the *static dynamics* method will be arbitrary, except being mutually orthogonal for each triplet of modes.

We now turn to a comparison of the analytical results to the results of a *static dynamics* (SD) analysis applied to simulation data for the Rouse model as described in the preceding section. The SD relaxation times shown in Fig. 2 agree perfectly with the spectrum of Rouse times given by Eq. (25) even for the highest mode numbers. The dataset which was used for the analysis consisted of 10 000 samples taken at time intervals of 100.0 which were generated by the

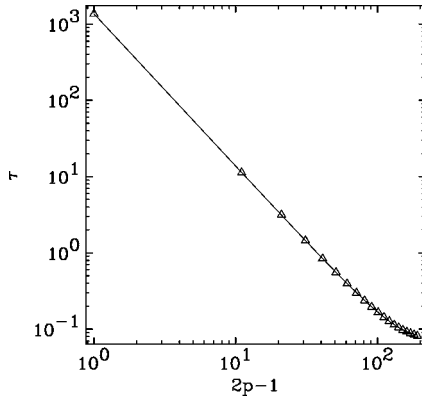


FIG. 2. Comparison of the relaxation spectrum of the Rouse chain calculated analytically from Eq. (25) and from simulation data by means of the *static dynamics* method (open triangles) for a chain with $N=100$ beads. Only every fifth value calculated from the data is shown to prevent cluttering of the symbols at large mode numbers p . At large p , there is a deviation from the scaling law $\tau \propto (2p-1)^2$, which is caused by the discreteness of the bead-spring chain.

Brownian dynamics simulation method described in Refs. [39,60]. An initial transient of 100 samples was discarded in order to eliminate effects of the initial configuration which was $\mathbf{R}_i = ib\hat{\mathbf{x}}$. After this period the distance between the two ends of the polymer had reached its equilibrium value of 10.0 within a statistical error of 2%. To obtain the above results we exploited the permutation symmetry of the coordinate axes and averaged τ_p and R_{pi} over the three coordinate directions $\hat{\mathbf{E}}^\alpha$. The values of the SD relaxation times obtained for the individual coordinate directions showed deviations of less than 5% from these averages. This deviation is approximately proportional to the size of the dataset. To get the same results without averaging, it was necessary to increase the size of the dataset by a factor of 4. If, on the other hand, only half of the data are used, the Rouse times of less than $\tau_p^R \approx 0.1$ were underestimated by the SD method. In the rest of this work, we will use ensembles of 5000–10 000 members and average over equivalent directions whenever possible.

The SD modes for $p=1,5,9$ are shown in Fig. 3 in comparison with the analytical results for the Rouse modes. We find that approximately the first 10% of the modes are reproduced accurately. For higher mode numbers, the tips of the sine waves are underestimated.

So far we have considered only a tethered polymer where all degrees of freedom relax. For a freely floating polymer, however, the center-of-mass motion is diffusive. This corresponds to an infinite relaxation time which spoils the numerics. The situation is easily remedied though, by performing the SD analysis on the bead positions *relative* to the center of mass. Thus, the relevant case for rheological applications can also be treated with the SD method.

V. APPLICATION TO NONLINEAR POLYMER MODELS AT EQUILIBRIUM

The knowledge of the equilibrium relaxation times of polymer models, taking into account excluded volume inter-

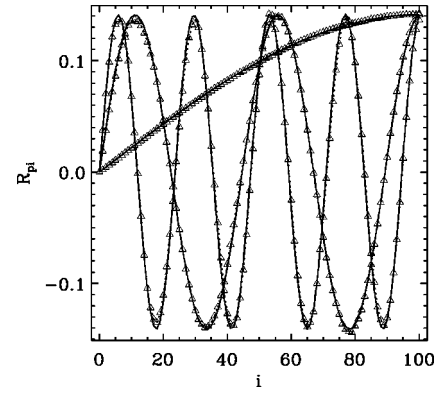


FIG. 3. Comparison of several Rouse modes ($p=1,5,9$) as calculated analytically from Eq. (26) (solid line) and from simulation data by means of the *static dynamics* method (open triangles) for a chain with $N=100$ beads.

actions (EVI) and hydrodynamics interactions (HI) between chain segments is summarized in scaling relations for the dependence of the longest relaxation time on the number of Kuhn segments, or beads, $\tau \propto N^\mu$. To this end, the longest relaxation time is estimated as the time the coil needs to diffuse its own size, i.e., $\tau_1 \approx R_E^2/D$ [14]. The static scaling relation $R_E \propto bN^\nu$, where $\nu=3/5$ with EVI and $\nu=1/2$ without EVI, relates the end-to-end distance R_E to the number of beads, N . Here, b is the length of a Kuhn segment, which corresponds to the root-mean-square bond length in the bead-spring model. The diffusion constant of the coil is $D \propto N\zeta$ or $D \propto 6\pi\eta R_E \propto 6\pi\eta bN^\nu$ in the free-draining and non-draining limits, corresponding to the cases without and with HI, respectively. Here, $\zeta=6\pi\eta a$ is the Stokes friction coefficient for a single bead of size a in a solvent of viscosity η . The results of this scaling theory agree with those obtained from the Rouse-Zimm model [11,12,61] which can be extended to account for EVI in an approximate way [15,62]. In addition, the latter also provides a scaling relation for the spectrum $\tau \propto (2p-1)^\theta$ and a numeric value for the longest relaxation time, given the bond length b and the bead friction coefficient ζ . Since it turns out that the exponents μ and θ , which give the dependence of the relaxation times on N and p , are the same, one may conclude that the p th mode describes the relaxation of subchains with N/p segments [15].

For the pure Rouse chain, the simple scaling theory gives $\tau_1 \propto N^2$. This result is also found from Eq. (25) when the expansion $\sin(x) \approx x$ is used, which is valid for $p \ll N$. For the Rouse chain with EVI and without HI one finds

$$\tau_1 \propto N^{2\nu+1} \approx N^{2.2}, \quad (27)$$

while for the Rouse model with both EVI and HI one has

$$\tau_1 \propto N^{3\nu} \approx N^{1.8}. \quad (28)$$

The results for the relaxation times corresponding to the latter two cases, as calculated from simulation data by the SD method, are shown in Fig. 4. The fit of a straight line to the data in the log-log plot indicates that the SD relaxation times do obey a power law for both models. The exponent obtained

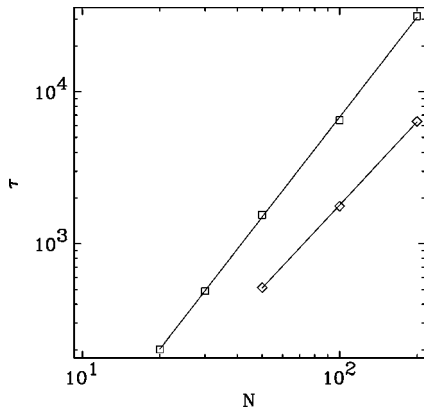


FIG. 4. Equilibrium scaling of the longest relaxation time with the number of segments for bead-spring chains with harmonic springs and excluded volume interactions (squares) and both excluded volume and hydrodynamic interactions (diamonds). The symbols give the values calculated from simulation data by the *static dynamics* method described in Sec. III. The solid lines are fits to a power law $\tau \propto \alpha N^\beta$, where the fit parameters are $\alpha = -0.55$ and $\beta = 2.19$ for the model with excluded volume interactions only and $\alpha = -0.40$ and $\beta = 1.83$ for the model with both excluded volume interactions and hydrodynamic interactions.

from the fit in the case with EVI only has a value of 2.19, which is in good agreement with the result 2.2 derived from scaling arguments. The fitted exponent in the case with both EVI and HI has a value of 1.83, which is again in good agreement with the scaling result of 1.8. Replacing the harmonic springs by finitely extensible nonlinear elastic (FENE) springs does not affect the scaling of the longest relaxation time with N as expected, since a change in the local interactions has no effect on the large scale behavior of the chain [15].

Figure 5 shows the full SD-relaxation spectra for different nonlinear bead-spring chains with $N=100$ beads. If FENE springs are used and other effects neglected (solid triangles), the SD times agree with the Rouse spectrum (solid line). Again, this is expected at least for the slow relaxation times. We find that agreement persists even for relaxation times where discreteness effects are already present. (Deviations for $p \geq 75$ are probably due to numerical errors because of the limited size of the dataset.)

Nonlocal interactions such as EVI, in contrast, do change the slow relaxation times. As observed in Fig. 5, adding EVI to the Rouse model (open squares) changes the scaling behavior from $\tau \propto (2p-1)^{-2}$ for the pure Rouse model to $\tau \propto (2p-1)^\theta$ with $\theta = -2.23$. For large values of p , there is a regime where no simple scaling law holds because of the discreteness of the chain. Furthermore, we find an overall increase of the relaxation times roughly by a factor of 5. The value of the longest relaxation time $\tau_1 = 6.50 \times 10^3$ is qualitatively consistent with a parallel study of polymer relaxation [63] where different aspects of the same model were considered. In that work an ensemble was prepared in an elongated nonequilibrium state and the time dependence of the x component of the end-to-end vector $\mathbf{R}_N - \mathbf{R}_0$ was recorded. The late stage of the relaxation, which corresponds to the linear regime where average perturbations and fluctuations relax in

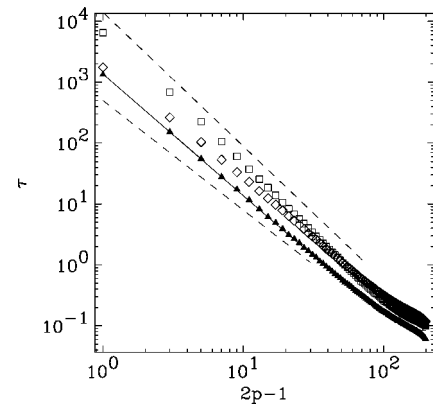


FIG. 5. Comparison of the spectra of relaxation times for several polymer models in thermal equilibrium. The solid line gives the analytical result for the discrete finite Rouse chain according to Eq. (25). The symbols give the values calculated from simulation data by the *static dynamics* approach described in Sec. III for bead-spring chains with harmonic springs and excluded volume interactions (open squares), chains with harmonic springs and both excluded volume and hydrodynamic interactions (open diamonds), and a FENE chain with no other interactions taken into account (solid triangles). The number of beads is $N=100$ in all cases. The dashed lines indicate the power laws with exponents -2.2 and -1.8 , obtained from scaling theory for chains with excluded volume interactions and without or with hydrodynamic interactions, respectively.

the same way, could be described as a single exponential decay with a time scale around $\tau \approx 6 \times 10^3$. This has the same order of magnitude as the SD relaxation time presented here and is also several times larger than the longest relaxation time of a Rouse chain which is $\tau_1^R = 1.36 \times 10^3$.

If HI are added to the Rouse model with EVI (open diamonds in Fig. 5), the scaling exponent θ calculated from a fit to the slow end of the spectrum is changed to $\theta = -1.78$. At intermediate values of p , it increases to $\theta = -1.97$ indicating that the HI acts less prominently over intermediate length scales. The value of the longest relaxation time $\tau_1 = 1.77 \times 10^3$ is decreased strongly compared to the Rouse model with only EVI. The value of the slowest SD relaxation time is again consistent with the time scale $\tau \approx 2 \times 10^3$ obtained from the time dependence of $\mathbf{R}_N - \mathbf{R}_0$ in Ref. [63].

Due to symmetry, in equilibrium the modes factorize in the same way as for the Rouse model also for nonlinear models. The form of the distance function R_{pi} , of course, may be different from that found for the Rouse model in Eq. (26). We find that EVI indeed leads to a change compared to the Rouse modes. The deviation is not large but clearly visible as shown in Fig. 6 for the first mode of a chain of $N=200$ beads. For higher modes, the difference with the Rouse modes is less pronounced. When HI is added or FENE springs are used, no difference compared to the Rouse form could be discerned.

VI. APPLICATION TO MODELS FOR DEFORMED TETHERED POLYMERS

Under the action of a force or flow, the beads in general have different nonzero average positions, $\langle \mathbf{R}_i \rangle \neq 0$, so that it

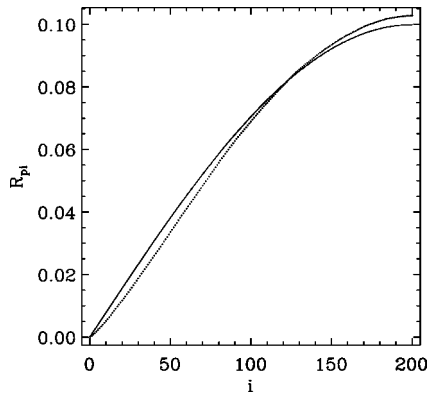


FIG. 6. First mode ($p=1$) in thermal equilibrium for the pure Rouse model (solid line) as calculated analytically in Appendix C and the model with harmonic springs and excluded volume interaction taken into account (dotted line) as calculated from numerical data by means of the *static dynamics* method. The chain length is $N=200$ in both cases.

becomes important to distinguish between the positions \mathbf{R}_i and the deviations $\mathbf{U}_i = \mathbf{R}_i - \langle \mathbf{R}_i \rangle$. The modes serve to decompose fluctuations, hence \mathbf{U}_p^α then gives the deviation of the true bead position from its mean value when the (p, α) mode is excited.

Moreover, when external forces or flows are present, the spherical symmetry of the equilibrium situation is broken. In the case of a force applied at the free end of the polymer or a uniform flow, one direction in real space, namely, that parallel to the force or flow, is distinguished. We refer to this as the *longitudinal* direction, while the other two directions, which are still related by a rotation symmetry, will be called *transverse*. Because of the reflection symmetry in the transverse directions, it is easy to see that cross correlations between one of these and the longitudinal direction must vanish. Therefore, the factorized form of the modes $\mathbf{U}_{pi}^\alpha = U_{pi} \hat{\mathbf{E}}^\alpha$ remains valid here.

Since the symmetry between the three coordinate directions is broken, one in general expects a “level splitting” of the relaxation times in each triplet, with one distinguished longitudinal relaxation time and two degenerate transverse relaxation times. Of course, in the numerical results the alignment of the mode directions parallel or perpendicular to the flow is not perfect. We distinguish the modes within each triplet on the basis of which of the components of their direction $\hat{\mathbf{E}}^\alpha$ has the largest value in a fixed coordinate system where the flow is along the x direction. Thus, the longitudinal mode is uniquely singled out. Differences between the transverse modes or their relaxation times—which should be equal by symmetry—may serve as an estimator for statistical errors in the results. In strong flows, there is also the possibility of “level crossing,” i.e., the triplets are no longer distinguished by large differences in the relaxation times. However, mode triplets can still be defined by the number of nodes of the distance function U_{pi} .

The Rouse model is the one exception to these general expectations. Due to linearity the equation of motion, Eq. (B12), may be split into an equation for the average $\langle \mathbf{R} \rangle$ and

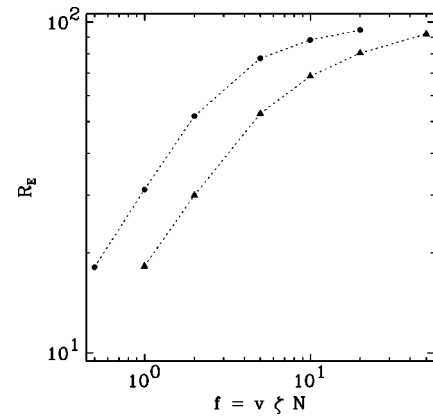


FIG. 7. End-to-end distance of a tethered FENE chain with $N=100$ beads pulled at its free end with different forces f (circles) and subjected to uniform flows of different velocities v (triangles). In the latter case, the total force exerted on the polymer, $v\zeta N$, is used to facilitate a comparison.

the deviation $\mathbf{R} - \langle \mathbf{R} \rangle$ from this average. The stochastic force is then seen to couple only to the latter, while the additional drag forces due to the flow appear only in the former. Therefore, only the average bead positions are affected by the flow and the relaxation times or modes do not change with flow velocity. This behavior is reproduced by the SD analysis.

Turning to a comparison of the two prototype situations of a tethered polymer pulled at the end and one which is subjected to a uniform flow, we first take a look at the polymer elongation in both cases. Since the strongest effect on the relaxation times turns out to be produced by the finite extensibility of the springs, we focus on a FENE chain with $N=100$ beads. In Fig. 7, the end-to-end distance is plotted as a function of the total force exerted on the polymer chain. In the end-pulled case (circles), this is simply the applied force f , while in the uniform flow case (triangles), for a free-draining polymer, the drag forces acting on each of the beads simply add up to a total force $f = v\zeta N$. From Fig. 7 it is seen that the uniform flow is less effective in stretching the polymer by a factor that is approximately constant, i.e., to achieve the same elongation requires a total force that is twice as strong.

The triplet of longest relaxation times for both cases is shown in Fig. 8 again as a function of the total force exerted on the polymer chain. For small f the relaxation times are close to their threefold degenerate equilibrium value. With increasing force, a strong decrease of all relaxation times is observed. The reason for this behavior is that the FENE springs become stiffer and stiffer the more they are stretched under the action of the external forcing. Furthermore, we find the expected level splitting, where the longitudinal mode relaxes faster than the transverse modes. The decrease of the longitudinal modes in both cases appears to follow a power law $\tau_1^\parallel \propto f^{-1.5}$. The decrease of the transverse modes is somewhat slower and may tentatively be described by $\tau_1^\perp \propto f^{-1.0}$. As for the polymer elongation the curves at large f differ only by an approximately constant factor rescaling the force. In the uniform flow case for $v \geq 0.2$, one even finds level crossing: The first longitudinal mode has only the fifth-largest

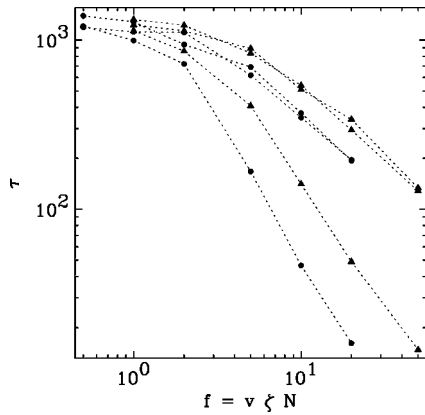


FIG. 8. The first triplet ($p=1$) of relaxation times as calculated by the *static dynamics* method from simulation data of a tethered FENE chain with $N=100$ beads pulled at its free end with different forces f (circles) and subjected to uniform flows of different velocities v (triangles). In the latter case, the total force exerted on the polymer, $v\zeta N$, is used to facilitate a comparison. The lower curve in each triplet corresponds to the longitudinal mode with direction along the flow for both cases.

relaxation time. This means that the transverse modes of the first two triplets relax slower than the slowest longitudinal mode.

While the qualitative behavior of the relaxation times is similar in both cases, the modes remain Rouse-like in the end-pulled case, but assume a completely different form in the uniform flow case as shown in Fig. 9 [72]. There, the first triplet of modes is shown for a force of $f=5.0$ in the end-pulled case (dotted lines) and a flow velocity of $v=0.2$ in the uniform flow case (dashed lines). These values have been

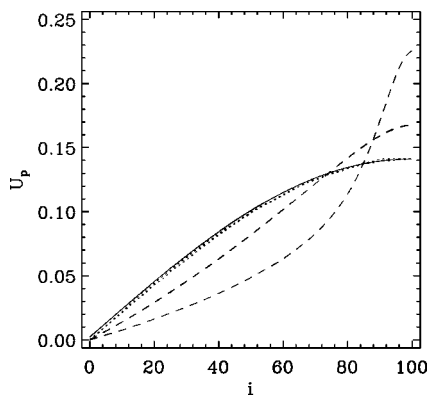


FIG. 9. The first triplet ($p=1$) of relaxation modes as calculated by the *static dynamics* method from simulation data of a tethered FENE chain with $N=100$ beads pulled at its free end (dotted lines) and subjected to a uniform flow (dashed lines). The values of the stretching force $f=5.0$ and flow $v=0.2$ are chosen so that the end-to-end distance of the polymer is comparable in both cases. For the end-pulled case, the shape of transverse and longitudinal modes is the same and agrees with the Rouse form (solid line). For the uniform flow case, the lower curve corresponds to the longitudinal mode, while the two upper curves represent the transverse modes, the symmetry between which is not broken. The shape of all modes in the triplet is quite different from the Rouse form.

chosen so that the polymer elongation is comparable in both cases. It corresponds to about 80% of the contour length Nb . For the polymer pulled at the ends, all three modes clearly have the Rouse form (solid line). When the polymer is subjected to a uniform flow, however, even the transverse modes are far from sinusoidal. This change of the shape of the modes is a consequence of the inhomogeneous distribution of tension along the chain [39]. In the end-pulled case, in contrast, the tension is the same everywhere along the chain.

We finally remark that for the number of beads considered here, $N=100$, adding EVI and HI to the FENE model does not significantly change the behavior of the relaxation times or modes. Chains with many more Kuhn segments, as they are used in experiments, are beyond the present simulation capabilities [39,60]. In this case, appreciable effects may occur.

VII. DISCUSSION AND CONCLUSIONS

The polymer relaxation spectrum forms an important link between the dynamics of single polymers and viscoelastic continuum mechanics. While for thermal equilibrium conditions a rather comprehensive theory is available, the relaxation behavior of deformed polymers is far less understood.

In the present work we have established an efficient method for calculating the complete polymer relaxation spectra and a set of corresponding modes from simulation data by employing the *static dynamics* approach. This approach rests on a relation for the initial decay rate which has been generalized here to nonequilibrium situations where detailed balance is valid. The latter has been shown to hold for polymers stretched by a force applied at the ends or by simple flow fields of either uniform or elongational type when a common averaging approximation is invoked to describe hydrodynamic interactions [12,34–37,49,51]. The relaxation modes are determined by the requirement that their initial decay is uncorrelated. In the linear case—where the conformational distribution function is Gaussian—this, of course, reduces to the usual Rouse modes, which are fully statistically independent. For nonlinear models the procedure amounts to using a generalized Rouse-Zimm model which is adapted to the simulation data.

The suggested procedure is subject to the general critique of any normal mode approach [14]. By its very construction it always yields $3N$ modes; the birth of new relaxation times as found in Ref. [64] or the possibility of a continuous relaxation spectrum conjectured in Ref. [14] is thus impossible within our framework. To circumvent the difficulties of the normal mode approach in the case of nonlinear polymer dynamics, the focus is usually shifted to the scaling behavior of the spectra. It was shown here that the equilibrium scaling exponents can also be obtained from the spectra calculated by the *static dynamics* method. In addition, the *static dynamics* method yields numeric values for the prefactors, which is important for technical applications, e.g., strong excluded volume interactions significantly slow down the relaxation process. Experimental evidence for a truly discrete spectrum has been given in Ref. [24].

The analysis of two simple nonequilibrium problems, a

tethered polymer pulled at its free end and a tethered polymer subjected to a uniform flow, revealed that it is important to correctly capture the nonlinear modes. In the uniform flow case, the finite extensibility of the polymer leads to a shape of the modes for a strongly stretched chain which is completely different from the Rouse form. In the end-pulled case, in contrast, the Rouse modes remain valid also for a strongly stretched chain. This latter case is untypical for polymers in flow in that the tension within the polymer is constant along its contour. In both cases, there is a strong velocity dependence of the relaxation times which decrease as the springs become harder the more the chain is stretched. This finding casts doubt [34,42] on the validity of theories for a coil-stretch transition in elongational flows [17,18] which assumed Rouse relaxation in the stretched state.

A large potential for further applications of the *static dynamics* method is to branched polymers and polymer networks where the calculation of relaxation times, even for simple Rouse-Zimm-like models can be quite tedious although possible analytically [65,66].

ACKNOWLEDGMENTS

We thank B. Dünweg and D. Kienle for stimulating discussions.

APPENDIX A: CONDITIONS FOR DETAILED BALANCE

Since the independent variables \mathbf{R}_i appearing in the Langevin equation (B12) are all even under time reversal, the condition for detailed balance is that for the stationary distribution \mathcal{P}_1^s the current defined in Eq. (12) vanishes [57,58], i.e.,

$$\mathbf{J}[\mathcal{P}_1^s] \equiv (\mathbf{v} + \mathbf{H} \cdot \mathbf{F}^\Phi) \mathcal{P}_1^s - k_B T \mathbf{H} \cdot \nabla \mathcal{P}_1^s = 0. \quad (\text{A1})$$

Dividing by \mathcal{P}_1^s and multiplying from the left by \mathbf{H}^{-1} yields

$$\mathbf{H}^{-1} \cdot \mathbf{v} + \mathbf{F}^\Phi = k_B T \nabla \ln(\mathcal{P}_1^s). \quad (\text{A2})$$

The right-hand side is explicitly gradient, hence, Eq. (A1) will be satisfied when a potential exists also for the left-hand side. This gives rise to the well-known potential condition [57,58]. Since here the direct force \mathbf{F}^Φ is already known to be derived from a potential, it remains to be shown that a potential exists also for $\mathbf{H}^{-1} \cdot \mathbf{v}$. This is the case when the matrix of derivatives, $\mathbf{D} = \nabla \otimes (\mathbf{H}^{-1} \cdot \mathbf{v})$, is symmetric. \mathbf{D} is an $N \times N$ supermatrix with components $\mathbf{D}_{ij} = \partial / \partial \mathbf{R}_j (\mathbf{H}_{ik}^{-1} \mathbf{v}_k)$, which are themselves 3×3 matrices. It will be symmetric when (i) the component-matrices \mathbf{D}_{ij} are symmetric and (ii) $\mathbf{D}_{ij} = \mathbf{D}_{ji}$. These two requirements are examined in the following. Throughout, summation over repeated indices will be implied.

To find conditions when the 3×3 component matrices \mathbf{D}_{ij} become symmetric, we first note that the imposed flow field at the position of the k th bead, of course, is a function of \mathbf{R}_k only, i.e., $\mathbf{v}_k = \mathbf{v}(\mathbf{R}_k)$. Hence,

$$\mathbf{D}_{ij} = \frac{\partial}{\partial \mathbf{R}_j} \mathbf{H}_{ik}^{-1} \mathbf{v}_k = \frac{\partial \mathbf{H}_{ik}^{-1}}{\partial \mathbf{R}_j} \mathbf{v}_k + \mathbf{H}_{ij}^{-1} \left. \frac{\partial \mathbf{v}}{\partial \mathbf{r}} \right|_{\mathbf{r}=\mathbf{R}_j}, \quad (\text{A3})$$

where $\partial \mathbf{v} / \partial \mathbf{r}$ is the velocity gradient of the imposed flow field. Clearly, in equilibrium, where $\mathbf{v} \equiv 0$, the rhs becomes zero which is trivially symmetric. In the free-draining limit, \mathbf{H}^{-1} is both conformation independent and diagonal, i.e., its component matrices are $\mathbf{H}_{ij}^{-1} = \delta_{ij} \zeta^{-1}$. Thus, \mathbf{D}_{ij} becomes symmetric when $\partial \mathbf{v} / \partial \mathbf{r}$ is symmetric. When an averaging approximation for the mobility matrix is invoked, then \mathbf{H}^{-1} becomes independent of the polymer conformation \mathbf{R} , but not diagonal. For the case of a uniform flow, where $\partial \mathbf{v} / \partial \mathbf{r} \equiv 0$, the trivial symmetry of \mathbf{D}_{ij} in Eq. (A3) then is immediately obvious. For the case of a constant but nonvanishing velocity gradient $\partial \mathbf{v} / \partial \mathbf{r} \equiv \text{const}$, which itself is symmetric, the following argument shows that the eigendirections of each component matrix of \mathbf{H} and \mathbf{H}^{-1} are the same as those of $\partial \mathbf{v} / \partial \mathbf{r}$. We choose orthogonal coordinates in real space along the eigendirections of $\partial \mathbf{v} / \partial \mathbf{r}$, which is possible by virtue of the assumptions made. Along each of these directions, there is a reflection symmetry so that upon averaging the conformation-dependent mobility supermatrix only those matrix elements which are even under each reflection do not vanish. In the Oseen approximation, Eq. (B8), these are precisely the diagonal elements of each 3×3 component matrix. Thus, it is seen that each of the averaged mobility component-matrices \mathbf{H}_{ij} has the same eigendirections as $\partial \mathbf{v} / \partial \mathbf{r}$. Since the component matrices of the inverse mobility are functions of those of the mobility itself, the former have again the same eigendirections as $\partial \mathbf{v} / \partial \mathbf{r}$. Hence, we conclude that \mathbf{H}_{ij}^{-1} is symmetric and commutes with $\partial \mathbf{v} / \partial \mathbf{r}$ so that again \mathbf{D}_{ij} as given by Eq. (A3) becomes symmetric.

Under the same conditions as above—averaged mobility matrix and constant symmetric velocity gradient—the requirement that the indices of the component matrix \mathbf{D}_{ij} can be interchanged simply becomes

$$\mathbf{H}_{ji}^{-1} \frac{\partial \mathbf{v}}{\partial \mathbf{r}} = \mathbf{H}_{ij}^{-1} \frac{\partial \mathbf{v}}{\partial \mathbf{r}}. \quad (\text{A4})$$

For the case of a uniform flow, $\partial \mathbf{v} / \partial \mathbf{r} \equiv \mathbf{0}$ so that this requirement is obviously satisfied. For the case of a constant but nonvanishing velocity gradient, $\partial \mathbf{v} / \partial \mathbf{r} \equiv \text{const}$, we have the fact that the supermatrix \mathbf{H}^{-1} is symmetric, i.e., its 3×3 component-matrices obey $\mathbf{H}_{ji}^{-1} = (\mathbf{H}_{ij}^{-1})^T$. As shown above, the component-matrices \mathbf{H}_{ij}^{-1} of the inverse averaged mobility supermatrix all have the same eigendirections as $\partial \mathbf{v} / \partial \mathbf{r}$ which implies $(\mathbf{H}_{ij}^{-1})^T = \mathbf{H}_{ij}^{-1}$. Hence, both sides of Eq. (A4) become equal. This completes the conclusion that detailed balance also holds for averaged hydrodynamic interactions when the velocity gradient is constant and symmetric.

To summarize, we have shown that detailed balance holds for an important class of polymer flow problems, where two conditions are met. The first condition is that the imposed flow be either constant everywhere $\mathbf{v} = \mathbf{v}_0$ or have a constant and symmetric gradient $\mathbf{v} = \kappa \mathbf{r}$. The former case of uniform flow has recently attracted great interest (see references cited in the Introduction) and is considered in Sec. VI of the

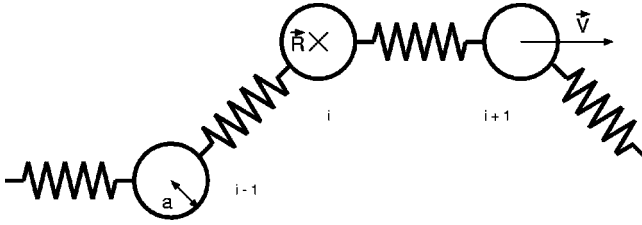


FIG. 10. Sketch of the bead-spring model for a polymer which is fixed at one end (bead index $i=0$) and free to move at the other (bead index $i=N$). The coordinate origin is arbitrarily chosen at the position of the fixed end. Also indicated are the bond length b and the effective hydrodynamic bead radius a .

present work. The latter case of elongational flow is important in rheology [1,2,23]. Second, the hydrodynamic interactions are described by an averaged mobility tensor which is a common practice in many studies of polymer dynamics, e.g., Refs. [12,34–37,49,51]. In more general situations, no obvious conclusions can be drawn, since an explicit expression for H^{-1} is not available (in contrast to H). We remark that external forces exerted on the polymer, e.g., by pulling the ends are subsumed in the direct force \mathbf{F}^Φ (in case they are derived from a potential which is generally the case). Since in this case $\mathbf{v}=\mathbf{0}$, detailed balance holds trivially.

APPENDIX B: BEAD-SPRING MODEL FOR NUMERICAL SIMULATIONS

For the numerical simulations we use a bead-spring model as sketched in Fig. 10. As usual, only motion on the diffusive time scale is considered, hence, the equation of motion for the position of the i th bead ($i=1, \dots, N$) is obtained from a balance between all forces acting on it. These forces comprise viscous drag forces \mathbf{F}^H on one side and potential and stochastic forces \mathbf{F}^Φ , \mathbf{F}^S on the other:

$$-\mathbf{F}_i^H = \mathbf{F}_i^\Phi + \mathbf{F}_i^S. \quad (\text{B1})$$

The potential force \mathbf{F}_i^Φ is often also called direct force to distinguish it from the solvent mediated hydrodynamic forces. It describes binding and excluded volume interactions between the beads as well as possible external forces applied, e.g., by laser tweezers, i.e.,

$$\mathbf{F}_i^\Phi = -\nabla_{\mathbf{R}_i}(\Phi^{\text{bond}} + \Phi^{\text{excluded}} + \Phi^{\text{ext}}). \quad (\text{B2})$$

The binding between next-nearest neighbors along the chain is described by either harmonic or FENE (finitely extensible nonlinear elastic) springs with potentials

$$\Phi^{\text{bond}} = \sum_{i=0}^{N-1} \frac{1}{2} k_H |\mathbf{R}_{i+1} - \mathbf{R}_i|^2 \quad (\text{B3})$$

or

$$\Phi^{\text{bond}} = \sum_{i=0}^{N-1} -\frac{1}{2} k_F R_F^2 \ln \left(1 - \frac{|\mathbf{R}_{i+1} - \mathbf{R}_i|^2}{R_F^2} \right), \quad (\text{B4})$$

respectively. For the case of harmonic springs, the force constant $k_H=3.0$ is chosen so that the root-mean-square bond length in equilibrium, b , becomes unity. The FENE spring law is augmented by a nearest-neighbor repulsion of the form described in Eq. (B6) below, so that a good approximation of rigid rods is obtained as described in Ref. [67]. Suitable parameter values for the force constant $k_F=30.0$ and the maximum extension of the spring $R_F=1.5$ result in a bond length of $b=0.96$ for this case. An additional bead with index $i=0$ which is fixed at $\mathbf{R}_0=0$ is used to implement the boundary condition at the tethered chain end. An external force with magnitude f and direction $\hat{\mathbf{x}}$ applied at the other chain end is considered in Sec. VI. The corresponding potential is

$$\Phi^{\text{ext}} = f \Theta[(\mathbf{r} - \mathbf{R}_N) \cdot \hat{\mathbf{x}}]. \quad (\text{B5})$$

The contribution arising from the excluded volume effect is purely repulsive and acts between any pair of beads. It is described by a truncated Lennard–Jones (LJ) potential

$$\begin{aligned} \Phi^{\text{excluded}} = & \sum_{\substack{j>i \\ i=1}}^N 4\epsilon \left(\left(\frac{\sigma}{|\mathbf{R}_j - \mathbf{R}_i|} \right)^{12} - \left(\frac{\sigma}{|\mathbf{R}_j - \mathbf{R}_i|} \right)^6 + \frac{1}{4} \right) \\ & \times \Theta(|\mathbf{R}_j - \mathbf{R}_i| - R_{\text{LJ}}). \end{aligned} \quad (\text{B6})$$

The parameters $\epsilon=1.0$ and $\sigma=1.0$ define energy and length scales of the excluded volume interaction. The cutoff radius $R_{\text{LJ}}=2^{1/6}\sigma$ is chosen at the minimum of the conventional Lennard-Jones potential and $\Theta(\mathbf{r})$ is the Heaviside function. When combined with harmonic springs, an effective equilibrium bond length of $b=1.33$ results [60]. Together with the FENE potential for the springs, the bead-spring chain becomes self-avoiding like a real polymer for the parameters chosen [67]. If the case without excluded volume effects is under investigation, Φ^{excluded} is set to zero.

The hydrodynamic forces are linear functions of the bead velocities $\dot{\mathbf{R}}_j$ relative to the imposed flow at their position, $\mathbf{v}(\mathbf{R}_j)$ [68]. In terms of the mobility matrix H , we have

$$\mathbf{F}_i^H = -\sum_{j=1}^N H_{ij}^{-1} \cdot [\dot{\mathbf{R}}_j - \mathbf{v}(\mathbf{R}_j)]. \quad (\text{B7})$$

Without hydrodynamic interactions, the inverse mobility matrix is proportional to the identity, $H^{-1}=\zeta\mathbf{1}$. The constant of proportionality is the single bead friction coefficient $\zeta=6\pi\eta a$, where η is the viscosity of the solvent and a is the effective hydrodynamic radius of a bead. Since in this case, the external flow remains unchanged throughout the polymer coil, this is referred to as the free-draining limit. If desired, hydrodynamic interactions are incorporated in the Oseen tensor approximation [15,69]. This turns the mobility into a conformation-dependent tensor, which is given by

$$H_{ij} = \begin{cases} \frac{1}{\zeta} & \text{for } i=j \\ \Omega(\mathbf{R}_i - \mathbf{R}_j) & \text{for } i \neq j, \end{cases} \quad (\text{B8})$$

where

$$\Omega(\mathbf{r}) = \frac{1}{8\pi\eta|\mathbf{r}|} (1 + \hat{\mathbf{r}}\hat{\mathbf{r}}^T) \quad (\text{B9})$$

is the Oseen tensor. Since the mobility matrix constructed with the Oseen tensor becomes nonpositive at small bead separations [23], we always consider hydrodynamic interactions together with the excluded volume effect. The collective effect of the HI is to reduce the penetration of the external flow into the polymer coil. The extreme case of this screening of the flow is referred to as the nondraining limit. To get a strong effect of HI, which in equilibrium comes as close as possible to the nondraining limit, we set $a/b = 0.25$. It should be noted, however, that parts of the polymer chain which become stretched under the action of an external force of flow eventually must become free draining [38].

A uniform flow field $\mathbf{v} = v\hat{\mathbf{x}}$ is considered specifically in Sec. VI, while homogeneous flows $\mathbf{v} = \mathbf{v}_0 + \kappa\mathbf{r}$ appear in the results of Sec. A.

The stochastic forces are related to the dissipative drag by the fluctuation dissipation theorem [70] to ensure the correct equilibrium distribution. Taking the forces acting on *all* beads together as a single supervector, we have

$$\mathbf{F}^S = \sqrt{2k_B T H^{-1}} \cdot \boldsymbol{\xi}, \quad (\text{B10})$$

where T is the temperature, k_B is the Boltzmann constant, and $\boldsymbol{\xi}$ is an uncorrelated Gaussian white noise with zero mean and unit variance

$$\langle \boldsymbol{\xi}(t) \rangle = \mathbf{0}, \quad (\text{B11})$$

$$\langle \boldsymbol{\xi}(t) \boldsymbol{\xi}^T(t') \rangle = \delta(t-t') \mathbf{1}.$$

In terms of the supervector \mathbf{R} for the bead positions, the equation of motion for the models considered may be written in the general form

$$\frac{\partial}{\partial t} \mathbf{R} = \mathbf{v}(\mathbf{R}) + \mathbf{H} \cdot (-\nabla_{\mathbf{R}} \Phi) + \sqrt{2k_B T \mathbf{H}} \cdot \boldsymbol{\xi}. \quad (\text{B12})$$

The potential Φ is obtained by summing the contributions from binding and excluded volume according to Eqs. (B3)–(B6), while the mobility is given by Eq. (B8). The yet unspecified parameters $k_B T = 1.0$ and $\zeta = 1.0$ essentially define the units of energy and time.

Except for the simple Rouse model \mathbf{v} , \mathbf{H} , and $\mathbf{F}^\Phi = -\nabla_{\mathbf{R}} \Phi$ are nonlinear functions of the polymer conformation \mathbf{R} , and one has to rely on numerical simulation to solve the equation of motion, Eq. (B12). A Brownian dynamics simulation scheme suitable for this task is described in Refs. [39,60].

APPENDIX C: THE ROUSE MODEL

Here, we consider a bead-spring chain of N beads connected by harmonic springs. For this case, Eq. (B12), which governs the Brownian dynamics of the chain reduces to the set of linearly coupled Langevin equations

$$\frac{\zeta}{k_H} \frac{\partial}{\partial t} \mathbf{R}_i = (\mathbf{R}_{i+1} - 2\mathbf{R}_i + \mathbf{R}_{i-1}) + \frac{\zeta}{k_H} \sqrt{2k_B T} \boldsymbol{\xi}, \quad (\text{C1})$$

where k_H is the force constant of the springs and ζ is the single bead friction coefficient. The bead index i runs from $i = 1, \dots, N$. In order to impose boundary conditions we introduce fictitious beads $i = 0, N+1$ where $\mathbf{R}_{0,N+1} = \text{const}$ for a fixed chain end and $\mathbf{R}_{0,N+1} = \mathbf{R}_{1,N}$ for a free-chain end. In the following, we will assume one end fixed at the origin and the other end free to move, i.e.,

$$\mathbf{R}_0 = \mathbf{0} \quad \text{and} \quad \mathbf{R}_{N+1} = \mathbf{R}_N. \quad (\text{C2})$$

Finding the general solution to Eq. (C1) requires diagonalization of the rhs, i.e., one has to solve the eigenvalue problem

$$\mathbf{R}_{i+1} - 2\mathbf{R}_i + \mathbf{R}_{i-1} = -\lambda \mathbf{R}_i. \quad (\text{C3})$$

The sign of λ is chosen such that positive eigenvalues yield stable solutions. Its relation to the relaxation time τ is

$$\tau = \frac{\zeta}{k_H} \frac{1}{\lambda}. \quad (\text{C4})$$

Equation (C3) has the form of a linear difference equation which may be solved by standard methods as described, e.g., in Ref. [71]. The ansatz $\mathbf{R}_k = \rho^k \hat{\mathbf{E}}^\alpha$, where $\hat{\mathbf{E}}^\alpha$ is the direction of the mode according to Sec. IV, leads to the auxiliary equation $\rho^2 - (2-\lambda)\rho + 1 = 0$, the solutions of which are

$$\rho_{1,2} = \frac{1}{2} [2 - \lambda \pm \sqrt{(2-\lambda)^2 - 4}]. \quad (\text{C5})$$

Depending on the sign of the radicand we have three different types of solution which are named analogous to their counterparts for differential equations although in the true sense of the word all solutions are, of course, bounded: (i) “unbound” solutions $R_k = c_1 \rho_1^k + c_2 \rho_2^k$ for $(2-\lambda)^2 > 4$; (ii) “secular” solutions $R_k = (c_1 + c_2 k) \rho^k$ for $(2-\lambda)^2 = 4$; and (iii) “bound” solutions $R_k = c_1 \cos k\theta + c_2 \sin k\theta$ for $(2-\lambda)^2 < 4$ [or equivalently $\theta \in (0, \pi)$].

In case (iii) we introduced θ by $(2-\lambda) = 2 \cos \theta$ which gives $\rho_{1,2} = \cos \theta \pm i \sin \theta$. Only this case leads to solutions which satisfy the boundary conditions under consideration [73]. For the constants c_1 and c_2 , we obtain from the boundary conditions

$$c_1 = 0, \quad c_2 \sin((N+1)\theta) = c_2 \sin(N\theta). \quad (\text{C6})$$

For $c_2 \neq 0$, one obtains

$$\theta = \frac{2p-1}{2N+1} \pi, \quad p = 1, 2, \dots, N. \quad (\text{C7})$$

Larger values of p violate the condition on θ . Hence, we obtain N eigenvalues

$$\lambda_p = 4 \sin^2 \left(\frac{2p-1}{2N+1} \frac{\pi}{2} \right). \quad (\text{C8})$$

The Rouse modes are then found by introducing this result in the ansatz in case (iii) as

$$\mathbf{R}_{kp} = c_2 \sin \left(k \frac{2p-1}{2N+1} \right). \quad (\text{C9})$$

The remaining constant $c_2 = 2/\sqrt{2N+1}$ is fixed by the normalization requirement $\sum_{k=1}^N \mathbf{R}_{kp}^2 = N$.

For boundary conditions with two free ends one obtains the results

$$\lambda_p = 4 \sin^2 \left(\frac{p}{N} \frac{\pi}{2} \right) \quad (\text{C10})$$

for the eigenvalues and

$$\mathbf{R}_{kp} = \frac{c_2}{\sin \theta/2} \cos \left[\left(k - \frac{1}{2} \right) \frac{p}{N} \pi \right] \quad (\text{C11})$$

for the eigenvectors. Here, p runs from $p=0, \dots, N-1$ and the normalization is $c_2 = 1/\sqrt{N}$.

If the argument of the sine in Eqs. (C8) and (C10) is small, one can expand the sine as $\sin(x) \approx x$. This reproduces the usual textbook result [15,59] for the different boundary conditions which is obtained by passing to a continuous version of Eq. (C1) at the very beginning of the calculation, whereby the finite difference operator $(\mathbf{R}_{i+1} - 2\mathbf{R}_i + \mathbf{R}_{i-1})$ is replaced by a second-order derivative. This is now seen to be an approximation which is valid if the mode number p is small compared to the number of beads N in the chain.

-
- [1] J.D. Ferry, *Viscoelastic Properties of Polymers* (John Wiley, New York, 1964).
- [2] R.B. Bird, R.C. Armstrong, and O. Hassager, *Dynamics of Polymeric Liquids*, 2nd ed. (Wiley, New York, 1987), Vol. 1.
- [3] H. Giesekus, *J. Non-Equilib. Thermodyn.* **11**, 157 (1986).
- [4] R.G. Larson, *Rheol. Acta* **31**, 213 (1992).
- [5] R.G. Larson, *Rheol. Acta* **31**, 497 (1992).
- [6] U.S. Agarwal, A. Dutta, and R.A. Mashelkar, *Chem. Eng. Sci.* **49**, 1693 (1994).
- [7] J.L. Lumley, *Annu. Rev. Fluid Mech.* **1**, 367 (1969).
- [8] P.S. Virk, *AIChE J.* **21**, 625 (1975).
- [9] A. Gyr and H.-W. Bewersdorff, *Drag Reduction of Turbulent Flows by Additives* (Kluwer Academic, Dordrecht, 1995).
- [10] A. Groisman and V. Steinberg, *Nature (London)* **405**, 53 (2000).
- [11] P.E. Rouse, Jr., *J. Chem. Phys.* **21**, 1272 (1953).
- [12] B.H. Zimm, *J. Chem. Phys.* **24**, 269 (1956).
- [13] B.H. Zimm, G.M. Roe, and L.F. Epstein, *J. Chem. Phys.* **24**, 279 (1965).
- [14] P.-G. de Gennes, *Scaling Concepts in Polymer Physics* (Cornell University Press, Ithaca, NY, 1981).
- [15] M. Doi and S. F. Edwards, *The Theory of Polymer Dynamics* (Clarendon Press, Oxford, 1986).
- [16] A. Onuki, *J. Phys. Soc. Jpn.* **54**, 3656 (1985).
- [17] P.-G. de Gennes, *J. Chem. Phys.* **60**, 5030 (1974).
- [18] E.J. Hinch, *Phys. Fluids* **20**, S22 (1977).
- [19] P.-G. de Gennes, *Physica A* **140**, 9 (1986).
- [20] R.B. Bird, R.C. Armstrong, and O. Hassager, *Dynamics of Polymeric Liquids, Vol. II: Kinetic Theory*, 2nd ed. (Wiley, New York, 1987).
- [21] R.G. Larson, *Constitutive Equations for Polymer Melts and Solutions* (Butterworth, Stoneham, MA, 1988).
- [22] L.G. Leal, in *Structure of Turbulence and Drag Reduction*, edited by A. Gyr (Springer, Heidelberg, 1990).
- [23] H.C. Öttinger, *Stochastic Processes in Polymeric Fluids* (Springer, Heidelberg, 1996).
- [24] T.T. Perkins, S.R. Quake, D.E. Smith, and S. Chu, *Science* **264**, 822 (1994).
- [25] T.T. Perkins, D.E. Smith, R.G. Larson, and S. Chu, *Science* **268**, 83 (1995).
- [26] S. Manneville, P. Cluzel, J.L. Viovy, D. Chatenay, and F. Caron, *Europhys. Lett.* **36**, 413 (1996).
- [27] S.R. Quake, H. Babcock, and S. Chu, *Nature (London)* **388**, 151 (1997).
- [28] P. Pincus, *Macromolecules* **9**, 386 (1976).
- [29] P. Pincus, *Macromolecules* **10**, 210 (1977).
- [30] F. Brochard-Wyart, *Europhys. Lett.* **23**, 105 (1993).
- [31] F. Brochard-Wyart, H. Hervet, and P. Pincus, *Europhys. Lett.* **26**, 511 (1994).
- [32] Y. Marciano and F. Brochard-Wyart, *Macromolecules* **28**, 985 (1995).
- [33] F. Brochard-Wyart, *Europhys. Lett.* **30**, 387 (1995).
- [34] J.W. Hatfield and S.R. Quake, *Phys. Rev. Lett.* **82**, 3548 (1999).
- [35] L. Harnau and P. Reineker, *New J. Phys.* **1**, 3.1 (1999).
- [36] R.G. Larson, T.T. Perkins, D.E. Smith, and S. Chu, *Phys. Rev. E* **55**, 1794 (1997).
- [37] B.H. Zimm, *Macromolecules* **31**, 6089 (1998).
- [38] R. Rzehak, D. Kienle, T. Kawakatsu, and W. Zimmermann, *Europhys. Lett.* **46**, 821 (1999).
- [39] R. Rzehak, W. Kromen, T. Kawakatsu, and W. Zimmermann, *Eur. Phys. J. E* **2**, 3 (2000).
- [40] C. Pierleoni, G. Arialdi, and J.-P. Ryckaert, *Phys. Rev. Lett.* **79**, 2990 (1997).
- [41] D. Kienle and W. Zimmermann, *Macromolecules* **34**, 9173 (2001).
- [42] R. Rzehak and W. Zimmermann, *Europhys. Lett.* **59**, 779 (2002).
- [43] H.C. Öttinger and W. Zylka, *J. Rheol.* **36**, 885 (1992).
- [44] Y. Rabin and J.W. Dash, *Macromolecules* **18**, 442 (1985).
- [45] P. Ahlrichs and B. Dünweg, *J. Chem. Phys.* **111**, 8225 (1999).
- [46] S.W. Provencher, *Comput. Phys. Commun.* **27**, 213 (1982).

- [47] C. Elster and J. Honerkamp, *J. Rheol.* **36**, 911 (1992).
- [48] B. Dünweg, M. Stevens, and K. Kremer, in *Monte Carlo and Molecular Dynamics Simulations in Polymer Science*, edited by K. Binder (Oxford University Press, Oxford, UK, 1995), Chap. 3.
- [49] B.H. Zimm, *Macromolecules* **13**, 592 (1980).
- [50] M. Fixman, *J. Chem. Phys.* **78**, 1588 (1983).
- [51] H.C. Öttinger, *J. Chem. Phys.* **86**, 3731 (1987).
- [52] R. Zurmühl and S. Falk, *Matrizen und Ihre Anwendungen* (Springer, Heidelberg, 1984).
- [53] R.A. Horn, *Matrices* (Cambridge University Press, Cambridge UK, 1985).
- [54] H. Goldstein, C. Poole, and J. Safko, *Classical Mechanics*, 3rd ed. (Addison-Wesley, Reading, MA, 2002).
- [55] R. Rzehak, *Eur. Phys. J. E.* (to be published).
- [56] H. Fischer and H. Kaul, *Mathematik für Physiker* (Teubner, Stuttgart, 1988), Vol. I.
- [57] C.W. Gardiner, *Handbook of Stochastic Methods* (Springer, Heidelberg, 1983).
- [58] H. Risken, *The Fokker-Planck Equation*, 2nd ed. (Springer, Heidelberg, 1989).
- [59] H. Yamakawa, *Modern Theory of Polymer Solutions* (Harper & Row, New York, 1971).
- [60] R. Rzehak, A. Arend, D. Kienle, and W. Zimmermann, in *Numerical Solutions of Polymer and Cell Dynamics*, edited by W. Alt, M. Chaplain, J. Griebel, and J. Lenz (Birkhäuser, Basel, 2003).
- [61] M.C. Williams, *J. Chem. Phys.* **42**, 2988 (1965).
- [62] N.W. Tschoegl, *J. Chem. Phys.* **40**, 473 (1964).
- [63] R. Rzehak, T. Kawakatsu, and W. Zimmermann (unpublished).
- [64] H.C. Öttinger, *J. Chem. Phys.* **90**, 463 (1988).
- [65] B.H. Zimm and R.W. Kilb, *J. Polym. Sci.* **37**, 19 (1959).
- [66] R.L. Sammler and J.L. Schrag, *Macromolecules* **21**, 1132 (1988).
- [67] K. Kremer and G.S. Grest, *J. Chem. Phys.* **92**, 5057 (1990).
- [68] R. Zwanzig, *Adv. Chem. Phys.* **15**, 325 (1969).
- [69] C. Pozrikidis, *Boundary Integral and Singularity Methods for Linearized Viscous Flow* (Cambridge University Press, Cambridge, UK, 1992).
- [70] H.C. Öttinger and Y. Rabin, *J. Rheol.* **33**, 725 (1989).
- [71] M.R. Spiegel, *Calculus of Finite Differences and Difference Equations* (McGraw-Hill, New York, 1971).
- [72] This figure corrects an erroneous normalization in Fig. 2 of Ref. [42].
- [73] Case (ii) arises for the center-of-mass motion of a free-Rouse chain.